Searching the mechanisms of mRNA buffering: the releasing-shuttling model

Qirun Wang[1] and Jie Lin[1,2]

[1] *Center for Quantitative Biology, Peking University, Beijing, China*
[2] *Peking-Tsinghua Center for Life Sciences, Peking University, Beijing, China*

(Dated: August 23, 2023)

Many experiments showed that eukaryotic cells maintain a constant mRNA concentration upon various perturbations by actively regulating transcription and degradation rates, known as mRNA buffering. However, the mechanism of mRNA buffering is still unknown. In this study, we propose a mechanistic model of mRNA buffering called the releasing-shuttling (RS) model. The model incorporates two crucial factors, X and Y, which play significant roles in the transcription, exportation, and degradation processes. The model successfully explains the constant mRNA concentration under genome-wide genetic perturbations and volume changes. Moreover, it quantitatively explains the slowed-down mRNA degradation after Pol II depletion and the temporal transcription dynamics after Xrn1 depletion. The RS model suggests that X and Y are likely composed of multiple molecules possessing redundant functions. We also present a list of potential X and Y candidates and an experimental method to identify X. Our work sheds light on a novel coupling mechanism between mRNA transcription, exportation, and degradation.

INTRODUCTION

Maintaining an appropriate mRNA level is vital for all living cells. Surprisingly, many eukaryotic cells adjust the mRNA production rate and the mRNA degradation rate to achieve a constant mRNA concentration, an elegant but mysterious phenomenon called mRNA buffering [1–3]. Numerous experiments carried out in the budding yeast *Saccharomyces cerevisiae* showed that the total mRNA concentration and also the mRNA concentrations of most individual genes are invariant against various perturbations, including genetic perturbations [4–14], and carbon source shift [15]. In cases where transcription-related genes are perturbed, the mRNA production rate decreases; interestingly, the mRNA degradation rate decreases accordingly so that the mRNA concentration is invariant. In cases where mRNA degradation-related genes are perturbed, the mRNA degradation rate drops, and the production rate decreases accordingly to maintain a constant mRNA concentration. Beyond the steady-state results, Chappleboim et al. recently showed that after an acute depletion of mRNA degradation factors, the mRNA degradation rate dropped immediately. However, the production rate decreased after a delay, so the total mRNA concentration temporarily accumulated and then gradually returned to its original level [16]. mRNA buffering phenomenon has been reported in mammalian cells as well [17, 18], suggesting its universality across eukaryotes. Strikingly, Berry et al. subjected mammalian cells to genome-wide genetic perturbation screening and found that the total mRNA concentration in both the nucleus and cytoplasm remained virtually unchanged despite a significant variation in the mRNA production rate [19].

Meanwhile, the total mRNA concentration and the mRNA concentrations of most genes are also constant as the cell volume increases [19–22]. The homeostasis of mRNA concentration in a growing cell volume is often considered a consequence of an mRNA production rate proportional to cell volume with a constant mRNA degradation rate [23, 24]. The volume-scaling mRNA production rate has been proposed to come from the limiting nature of Pol II [25, 26] – the mRNA production rate is proportional to the copy number of RNA polymerase II (Pol II), which is proportional to the cell size. However, Swaffer et al. recently found that the mRNA production rate increases sublinearly with the cell volume in *Saccharomyces cerevisiae*. Surprisingly, the mRNA degradation rate decreases accordingly and perfectly balances the mRNA production rate so that the mRNA concentration remains constant [27].

In all the above examples, a coupling between mRNA production and mRNA degradation exists and balances the two rates so that the mRNA concentration is constant. It has been suggested that mRNA feedback to its own production or degradation may lead to mRNA buffering [16, 19, 27]. In addition to mRNA itself, several proteins have been suggested as possible players in mRNA buffering. One noteable protein is Xrn1, the 5'-3' exonuclease that plays a crucial role in cytoplasmic mRNA degradation. Recent studies have shown that it also shuttles into the nucleus and functions in transcription regulation, suggesting its potential role in connecting mRNA production and degradation [8, 9, 28–30]. Similarly, the Ccr4-Not complex involved in mRNA deadenylation has also been found to shuttle between cytoplasm and nucleus and regulate transcription [31]. Other examples include Snf1, the yeast ortholog of AMP-activated protein kinase (AMPK), which interacts with both degradation machinery and transcription factors [32], and Rpb4/7, which are subunits of Pol II and participate in both transcription and degradation of certain mRNAs [33–35]. All these factors share two common features: they play a role in both transcription

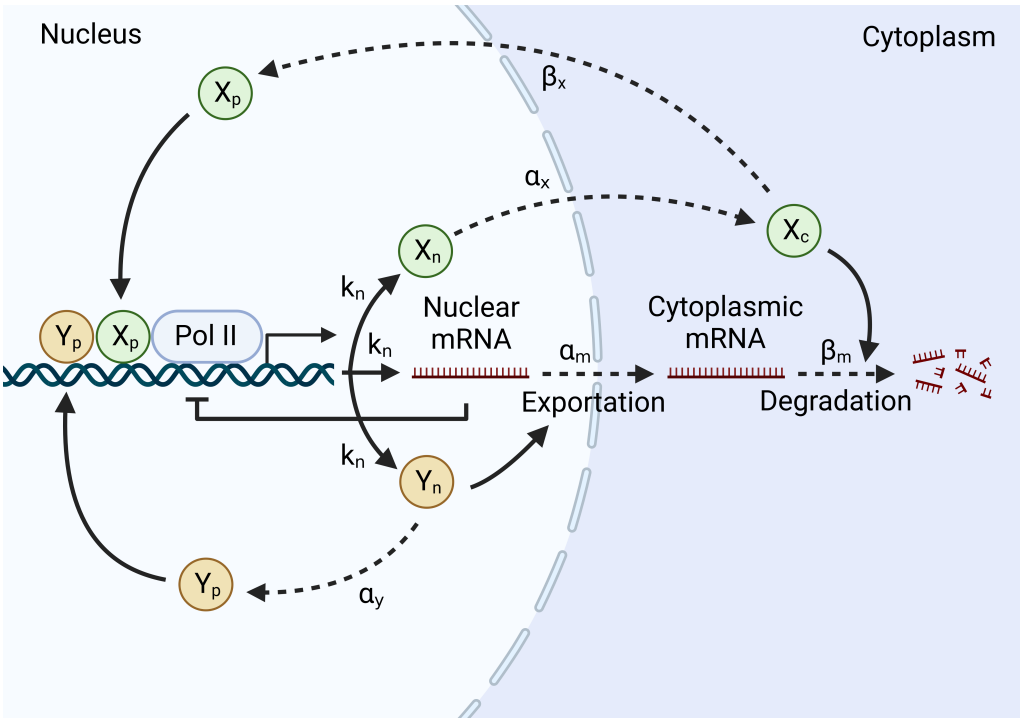

FIG. 1. **Schematic of the releasing-shuttling model.** One copy of protein X and Y in the activated states (X_n and Y_n) are released after each transcription initiation. k_n is the mRNA production rate, which is also the rate of transcription initiation. X_n transitions to the cytoplasm with a constant rate α_x and becomes X_c, which degrades mRNAs with a rate proportional to the constant β_m. X_c has a constant rate β_x to shuttle back to the nucleus and becomes X_p. Y_n exports nuclear mRNAs to the cytoplasm with a rate proportional to the constant α_m. Y_n transitions to the inactivated state Y_p with a constant rate α_y.

and mRNA degradation and can shuttle between nucleus and cytoplasm to transmit information along the mRNA metabolic pipeline. These features are necessary to connect transcription and degradation in mRNA buffering.

Despite extensive knowledge of molecular details that may contribute to mRNA buffering, its mechanism remains mysterious. In this work, we provide the first mechanistic model of mRNA buffering (as far as we realize) that can explain and unify multiple experimental observations of mRNA buffering. In this work, we mainly study the total concentration of all mRNAs, which we call the mRNA concentration in the following unless otherwise mentioned. Our conclusions regarding mRNA buffering do not necessarily apply to all individual genes since they can be under specific regulations [8, 9, 19]. In particular, we have shown before that the promoter strength of a gene may make its mRNA and protein concentration exhibit nonlinear scaling with cell volume [26]. In the following, we show that models involving mRNA feedback to its own production or degradation cannot achieve robust mRNA buffering. We then introduce the minimal mechanistic model of mRNA buffering, the releasing-shuttling (RS) model. The critical ingredients of the RS model are two proteins, X and Y, released after each transcription initiation. Protein X, responsible for mRNA degradation, is exported to the cytoplasm and shuttles back to the nucleus. Protein Y is responsible for the export of mRNA to the cytoplasm. We demonstrate how the RS model quantitatively explains multiple experimental observations and makes experimentally testable predictions. Finally, we identify candidates for the key proteins X and Y, and discuss possible extensions of the RS model.

RESULTS

The releasing-shuttling (RS) model

It has been suggested that a negative feedback of mRNA to its own production or a positive feedback to its own degradation can be potential mechanisms of mRNA buffering [16, 19, 36]. However, we found that the feedback models generally cannot lead to robust buffering. Changing the mRNA production or degradation rates always leads to a significant change in the mRNA concentration (Supplementary Information and Figure S1). In contrast, the mRNA concentration was largely invariant to these perturbations in experiments [8, 9]. In particular, the mRNA concentration and production rate appeared uncorrelated across genome-wide perturbations in mammalian cells [19].

In the following, we introduce a minimal mechanistic model of mRNA buffering with two essential proteins, X and Y (Figure 1). X is a degradation factor that shuttles between the nucleus and the cytoplasm. Y functions in mRNA export and is localized in the nucleus. X can be in three states: the activated state in the nucleus that is just released from transcription initiation and ready to be exported to the cytoplasm (X_n), the inactivated state in the nucleus that is essential for transcription initiation (X_p), and the cytoplasmic state responsible for mRNA degradation (X_c). Y can be in two states: the activated state in the nucleus just released from transcription initiation (Y_n) and the inactivated state in the nucleus essential for transcription initiation (Y_p).

Below, we summarize the key ingredients of the RS model necessary to achieve mRNA buffering in the nucleus and cytoplasm:

- Proteins X and Y are necessary for transcription initiation. They bind to the preinitiation complex (PIC) as X_p and Y_p and get released as X_n and Y_n after each transcription initiation.
- Binding between nuclear mRNAs to Y_n is the limiting step of mRNA export.
- Binding between cytoplasmic mRNAs to X_c is the limiting step of mRNA degradation.

The first ingredient is justified by the fact that transcription initiation is a step-by-step process propelled by different functional groups, which sequentially bind and leave the transcription machinery. In particular, the carboxyl-terminal domain (CTD) region of Pol II is a versatile harbor providing numerous docking points for proteins functioning in diverse processes such as initiation-to-elongation transformation and mRNA processing [37]. We suppose proteins X and Y are two of the signaling molecules that are released during transcription initiation. The second ingredient is supported by recent studies showing that mRNA export is under sophisticated regulations [38, 39]. Interestingly, transcription has been shown to be necessary for mRNA export [40], supporting our model assumption. We hypothesize that protein Y in the state Y_n is an export regulator of mRNA. The third ingredient is supported by multiple pieces of evidence showing that cytoplasmic degradation factors of mRNA shuttles in and out of the nucleus and appear critical for transcription [8, 9, 14, 31–33].

The mathematical equations of the RS model are the following,

$$\frac{dm_n}{dt} = k_n - \alpha_m \frac{Y_n}{V_n} m_n, \tag{1}$$

$$\frac{dX_n}{dt} = k_n - \alpha_x X_n, \tag{2}$$

$$\frac{dY_n}{dt} = k_n - \alpha_y Y_n, \tag{3}$$

$$\frac{dm_c}{dt} = \alpha_m \frac{Y_n}{V_n} m_n - \beta_m \frac{X_c}{V_c} m_c, \tag{4}$$

$$\frac{dX_c}{dt} = \alpha_x X_n - \beta_x X_c, \tag{5}$$

$$\frac{dX_p}{dt} = \beta_x X_c - k_n, \tag{6}$$

$$\frac{dY_p}{dt} = \alpha_y Y_n - k_n. \tag{7}$$

Here m_n is the number of nuclear mRNAs, and m_c is the number of cytoplasmic mRNAs. k_n is the mRNA production rate, which depends on multiple factors, including the concentrations of Pol II, X_p, and Y_p. V_c is the cytoplasmic volume, and V_n is the nuclear volume that is proportional to V_c [41]. The binding rate of mRNA to Y_n is proportional to its concentration with a factor α_m, which is the limiting step of mRNA export. α_x quantifies how fast X_n escapes the nucleus, and α_y quantifies how fast Y_n transforms back to Y_p. Similarly, the binding rate of mRNA to X_c is proportional to its concentration with a factor β_m. β_x quantifies how fast X_c shuttles back to the nucleus.

It is straightforward to find the steady-state solution of the RS model:

$$m_n = \frac{\alpha_y}{\alpha_m} V_n, \tag{8}$$

$$m_c = \frac{\beta_x}{\beta_m} V_c, \tag{9}$$

$$X_n = \frac{k_n}{\alpha_x}, \tag{10}$$

$$X_c = \frac{k_n}{\beta_x}, \tag{11}$$

$$Y_n = \frac{k_n}{\alpha_y}. \tag{12}$$

Intriguingly, the numbers of nuclear and cytoplasmic mRNAs are proportional to the nuclear and cytoplasmic volumes, respectively. These are necessary conditions for any model to be biologically valid: the model must predict a constant mRNA concentration. Further, the nuclear and cytoplasmic mRNA concentrations are independent of the mRNA production rate k_n and protein X and Y copy numbers! The nuclear and cytoplasmic mRNA concentrations only depend on the microscopic parameters α_m, α_x, β_m, and β_x, which we propose are set by physical processes and hardly affected by genetic perturbations. According to the RS model, the validity of mRNA buffering is independent of the mechanisms that

set the mRNA production rate. The trick is that the information on the mRNA production rate is conveyed through the concentrations of Y_n, X_n, and X_c, which synchronizes the speed of mRNA export and degradation so that m_n and m_c are independent of k_n. To ensure their concentrations are proportional to k_n, we concluded that proteins X and Y must be necessary for transcription initiation; otherwise, mRNA buffering is invalid. To explicitly demonstrate this point, we introduced a modified model in which proteins X and Y are not necessary factors to initiate transcription and found that mRNA buffering in this modified model does not hold (Supplementary Information and Figure S2). Also, the nuclear localization of protein Y is not critical for our conclusions. In a modified model in which Y is exported out of the nucleus with rate α_y and then shuttles back with rate β_y, mRNA buffering is still valid (Supplementary Information and Figure S3).

The RS model predicts mRNA buffering against various genetic perturbations

The RS model shows that the validity of mRNA buffering does not require a particular form of the mRNA production rate k_n since it does not enter the expressions of m_n and m_c. Nevertheless, starting with a biologically valid model for transcription makes it possible to compare theories with experiments explicitly, as we show later. Therefore, we incorporated several general features of transcription regulation into the RS model. First, the copy number of Pol II is often limiting for transcription, supported by multiple experiments [22, 23, 36]. Because the Pol II copy number is proportional to the nuclear volume [36], we used the nuclear volume as a proxy for Pol II. It has been found that the number of actively transcribing Pol II increases sublinearly with the total Pol II number given fixed gene copy numbers [27], presumably due to the finite DNA substrates for Pol II to bind [26]. Therefore, we modeled the effects of limiting Pol II resource through an mRNA production rate that is a Hill-function of the nuclear volume, which saturates for a large nuclear volume given a fixed amount of DNA. Second, the nuclear mRNAs have negative feedback to their own production [19, 42] although the detailed mechanisms are still unclear. To sum up, we proposed the following form of the mRNA production rate,

$$k_n = k_0 \frac{V_n}{V_n + K_v} \frac{K_m}{c_{m,n} + K_m} \frac{x_p}{x_p + K_x} \frac{y_p}{y_p + K_y}. \quad (13)$$

The first term on the right side of Eq. 13 represents the sublinear volume dependence of actively transcribing Pol II. The second term represents the negative feedback of nuclear mRNA to transcription where $c_{m,n} = m_n/V_n$. Finally, the last two terms represent the binding probabilities of X_p and Y_p to PIC where x_p and y_p are the nulcear concentrations of X_p and Y_p respectively: $x_p = X_p/V_n$ and $y_p = Y_p/V_n$. In the steady state, given the total copy number of protein X (X_t) and the total copy number of protein Y (Y_t), X_n, X_p, X_c, Y_n and Y_p can be found through the conservation equations, $X_t = X_n + X_c + X_p$, $Y_t = Y_n + Y_p$. Here, $X_n = k_n/\alpha_x$, $X_c = k_n/\beta_x$, $Y_n = k_n/\alpha_y$, and k_n is a function of X_p and Y_p via Eq. 13.

To mimic genome-wide genetic perturbations similar to previous experiments [8, 9, 19], we systematically perturbed the parameters in the RS model including k_0, K_v, K_x, K_m, K_y, V_n, and V_c in Eq. 13, as well as X_t and Y_t (see details of numerical calculations in Methods). According to the RS model, all the perturbations may change the mRNA production rate but should leave the nuclear and cytoplasmic mRNA concentrations invariant. Indeed, we found that the simulated data nicely matched the experimental data (Figure 2a, b, d, and e) [19], both exhibiting a virtually zero correlation between the mRNA production rate and the mRNA concentrations. In Figure 2a, b, d, and e, the blue dashed lines are $x = 1$ lines, while the red dashed lines are from solving the RS model numerically with different α_m, which we explain in the next section.

In Ref. [9], Sun et al. measured the mRNA production rate and degradation rate and found an approximately linear relation between these two rates across 46 yeast deletion strains, which suggested mRNA buffering (Figure 2c). To further verify the RS model, we plotted the mRNA production rate vs. the mRNA degradation rate from the same simulations as Figure 2d, e. We also found a linear relationship between them (Figure 2f) in concert with experiments.

In this work, we used a set of basic parameters (Table II) for all simulations unless otherwise mentioned (Methods). The basic parameters were from the fitting of kinetic data of budding yeast (Figure 4a) with the MM constant K_v inferred from the experimental data of mRNA production rate vs. cell volume (Figure 3b), which we explain in later sections. These parameters are presumably different from mammalian cells. Nevertheless, using the set of basic parameters and only adjusting the k_0 value in Eq. 13, we found that the simulations and experimental data already quantitatively agreed in Figure 2. In summary, our conclusions regarding the robustness of mRNA buffering are insensitive to the parameters.

The RS model predicts when mRNA buffering break downs

Experimentally, violations of nuclear mRNA buffering were observed when the export of nuclear mRNA was impaired [19]. Intriguingly, the RS model also predicts the breakdown of nuclear mRNA buffering. Specifically, the RS model predicts that when nuclear mRNA export

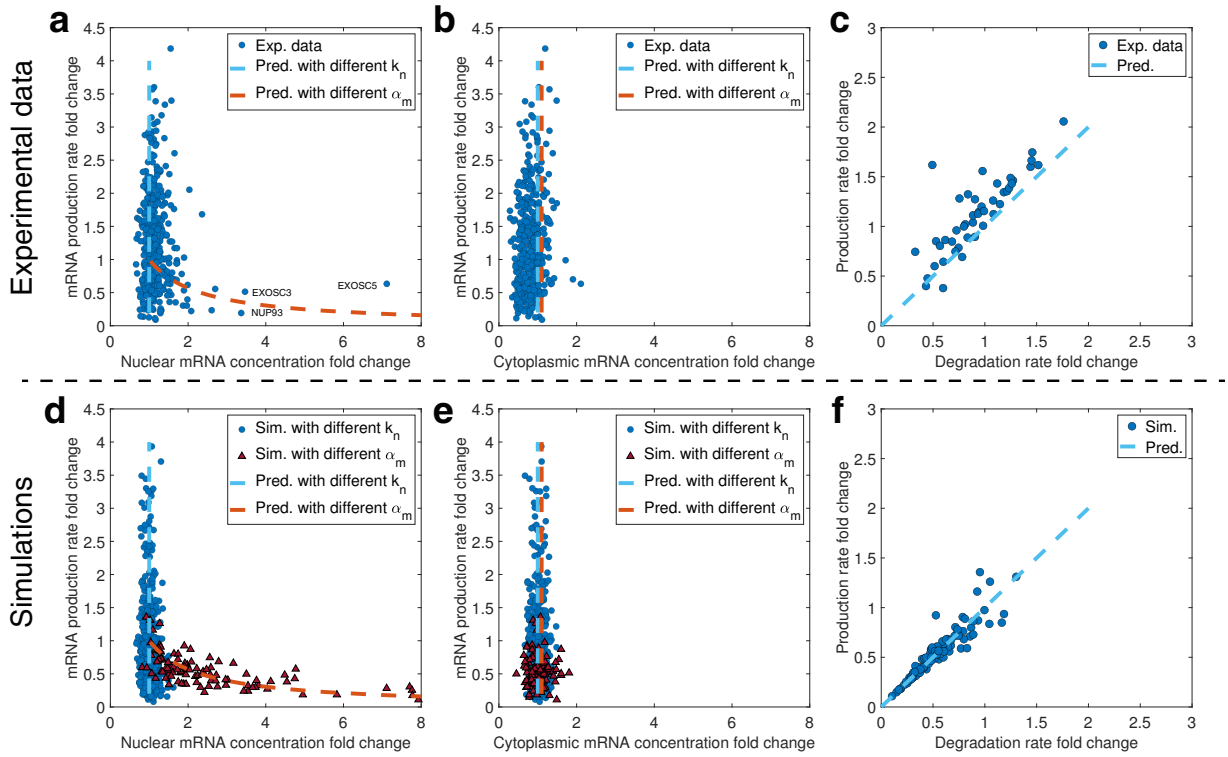

FIG. 2. **The RS model predicts mRNA buffering against genetic perturbations.** (a) Experimental data from Ref. [19] show that the nuclear mRNA concentration is buffered against changes in the mRNA production rate (Methods). Each data point represents a knockdown of a particular gene with the three genes EXOSC3, EXOSC5, and NUP93 highlighted. The blue dashed line is an $x = 1$ line, and the red dashed line represents the prediction when α_m is perturbed. The same meanings of dashed lines apply to (b, d, e). (b) Experimental data from Ref. [19] show that the cytoplasmic mRNA concentration is buffered against changes in the mRNA production rate. (c) Experimental data of the mRNA production rate vs. the degradation rate from Ref. [9]. The blue dashed line is a $y = x$ line. (d) Simulations of the RS model show that the nuclear mRNA concentration is buffered against changes in the mRNA production rate. The blue circles represent simulation results with multiple parameters perturbed and the red triangles represent simulation results with α_m perturbed. The same meanings of points apply to (e). We randomly sampled the mRNA copy numbers from a Poisson distribution with the means equal to the predictions of the RS model, mimicking gene expression noise. We also added Gaussian noise on top of the mRNA production rates so that the CVs are equal to 0.05. The same noises were applied to (e). (e) Numerical data of the RS model show that the cytoplasmic mRNA concentration is buffered against changes in the mRNA production rate. (f) Numerical data of the mRNA production rate vs. the degradation rate from the RS model. The blue dashed line is a $y = x$ line. Data are from the same simulations of (d, e). For both the production rates and degradation rates, we added Gaussian noises on top of them so that the CVs are equal to 0.05.

is impaired, that is, a lower α_m in the RS model (Eq. 8), the nuclear mRNA concentration is not constant anymore but negatively correlates with the mRNA production rate. In Figure 2a and d, the red dashed lines were from the numerical calculations of the RS model with changing α_m. The red triangles in Figure 2d were obtained by randomly sampling α_m (see details of numerical calculations in Methods). In the RS model, the negative correlation between the mRNA production rate and the nuclear mRNA concentration comes from the negative feedback from the nuclear mRNA concentration to the mRNA production rate, and we confirmed this by showing that the negative correlation is absent in a modified model without this negative feedback (Figure S4). Intriguingly, the RS model predicts that the cytoplasmic mRNA concentration is uninfluenced by the impairment of nuclear mRNA export (Eq. 9), which exactly matches the experimental observations (Figure 2b and e).

Biologically, nuclear mRNA export needs accurate mRNA processing and the proper assistance of multiple structures like nuclear pores [43]. The RS model successfully explains the breakdown of nuclear mRNA buffering when the nuclear pore component NUP93 and the core components of the nuclear RNA exosome EXOSC3 and EXOSC5 are knocked down [19], strongly supporting that the RS model captures the key ingredients of mRNA buffering.

The RS model leads to mRNA buffering as the cell volume increases

We then sought to test if the RS model can achieve homeostasis of mRNA concentration during cell growth (Figure 3a). For simplicity, we assumed that the total copy numbers of proteins X and Y are proportional to the cell volume, which is valid for most proteins [44]. We first fit the experimental data of mRNA production rate vs. cell volume from Ref. [27] using Eq. 13 assuming a constant ratio between the total cell volume and nuclear volume (the blue line in Figure 3b). From this fitting, we obtained the value of K_v for WT cells. K_v and other parameters inferred from the fitting of kinetic data of budding yeast (see the next section) constitute the basic parameters in this work (Methods and Table II). In the above fitting, we neglected the volume dependence of x_p and y_p and confirmed that this approximation was valid (Figure S5). The nuclear mRNA concentration $c_{m,n}$ is also constant in Eq. 13 due to mRNA buffering, as shown in the following.

We defined the mRNA degradation rate δ_m as the degradation rate per mRNA, i.e., $\delta_m = \beta_m X_c/V_c$ according to Eq. 4. Therefore, the mRNA lifetime $\tau_m = 1/\delta_m$. Notably, the predicted mRNA degradation rate from the RS model (the red line in Figure 3b) precisely matches the experimentally measured values (red triangles) without any fitting parameters. Within the RS model, while the mRNA production rate scales sublinearly with the cell volume, the degradation rate decreases accordingly to achieve a constant mRNA concentration (Figure 3b). The RS model shows that the mRNA degradation rate automatically compensates for the sublinear mRNA production rate, consistent with experiments. In fact, according to the RS model, any cell-volume dependence of the mRNA production rate will lead to a constant mRNA concentration. We confirmed this prediction by assuming an mRNA production rate that is a superlinear (Figure 3c) or oscillating (Figure 3d) function of cell volume. In both cases, the mRNA degradation rate self-adjusts to compensate for the mRNA production rate and generates a constant mRNA concentration. This stringent prediction can be tested experimentally.

Slowed mRNA degradation after Pol II depletion

In Ref. [36], Swaffer et al. depleted half of Pol II in budding yeast and measured the degradation of a particular gene's mRNA. They found that mRNA degradation slowed down after Pol II depletion. We found that this experimental observation is a direct consequence of the RS model. According to the RS model, the mRNA degradation rate should decrease if the mRNA production rate decreases. Because the Pol II copy number is proportional to the nuclear volume, reducing the Pol II concentration to its half value is equivalent to doubling the MM parameter K_v in Eq. 13. Once the mRNA production rate decreases due to Pol II depletion, more X_c shuttles from the cytoplasm to the nucleus to become X_p, leading to slowed mRNA degradation.

To verify our idea, we numerically simulated a slightly modified model in which we separated the transcription of a single gene from the rest of the genome. We monitored the time-dependence of the mRNA number of the particular gene (including both the nuclear and cytoplasmic mRNA) after turning off its transcription. We first fitted the data of mRNA production rate vs. cell volume before Pol II depletion by optimizing parameters except K_v in the set of basic parameters (blue lines and circles in Figure 3e, and Methods). We then doubled K_v to model Pol II depletion. We found that the RS model nicely predicts the slowed mRNA degradation after Pol II depletion without further fitting (Figure 3e).

Temporal transcription dynamics after rapid degradation of protein X

In Ref. [16], Chappleboim et al. rapidly depleted Xrn1 in budding yeast and monitored the temporal dynamics of the total mRNA concentration and the level of recently transcribed mRNA, which is a good proxy for the mRNA production rate. Experimental observations revealed three phases of mRNA dynamics upon the sudden removal of the protein Xrn1 (Figure 4a). In the accumulation phase, the mRNA concentration increased, and the mRNA production rate remained almost constant. In the adaptation phase, the mRNA production rate dropped rapidly, and the mRNA concentration ceased to increase. In the reversion phase, the mRNA production rate decreased and approached the new steady-state value, and the mRNA concentration gradually reduced to its original value before the depletion of Xrn1. To verify whether the RS model can explain the temporal dynamics of mRNA as a more stringent test, we studied the RS model after a rapid depletion of protein X.

First, we remark that in the RS model, protein X is presumably a coarse-grained combination of several proteins. This idea is supported by the experimental observations that mRNA buffering was still valid even if Xrn1 was knocked out [8, 16], which we discuss in detail later. Therefore, the depletion of Xrn1 should correspond to a partial depletion of protein X in the RS model. Given that Xrn1 is the primary degradation factor in budding yeast [8] and more than 90 percent copies of Xrn1 are localized in the cytoplasm [45], we modeled the depletion of Xrn1 as a rapid reduction of X_c to its 20% value in the cytoplasm.

Due to the much lower value of X_c, the replenishment of X_p (Eq. 6) significantly decreases (Figure 4b). However, there is a delay between the decrease in the mRNA

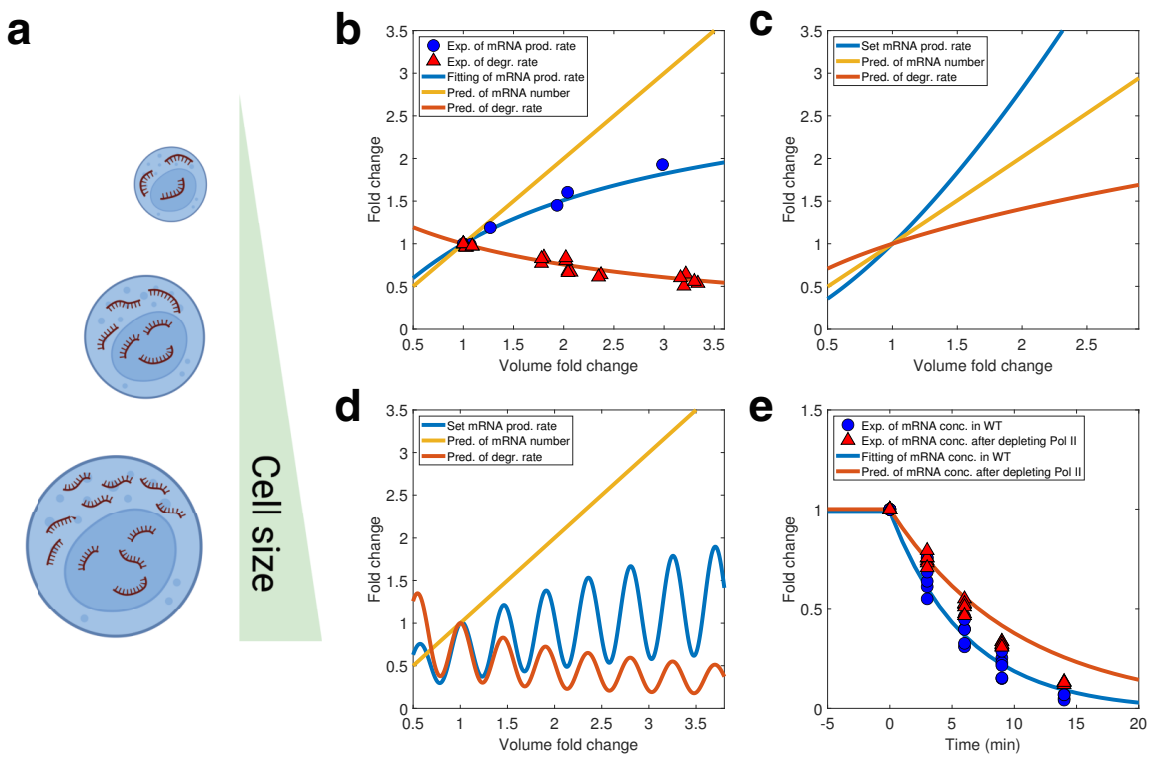

FIG. 3. **The RS model predicts mRNA buffering during cell growth and slowed mRNA degradation after Pol II depletion.** Exp., experiment; Pred., prediction. (a) Schematic showing the homeostasis of mRNA concentration during cell growth. (b) Experimental data from Ref. [36] for the mRNA production rate, degradation rate, and the mRNA number as a function of cell volume during cell growth. The blue line is a fitting of the experimental data ($r^2 = 0.98$). The red line is the predicted mRNA degradation rate per mRNA without any fitting parameters from the RS model. The yellow line is the predicted mRNA copy number. (c) mRNA buffering occurs even if the mRNA production rate exhibits a superlinear scaling with cell volume. In this case, the mRNA degradation rate increases with the cell volume accordingly to make the mRNA concentration constant. (d) mRNA buffering occurs even if the mRNA production rate oscillates with cell volume. In this case, the mRNA degradation rate also oscillates, and the mRNA concentration remains constant. (e) The normalized mRNA concentration for a particular gene following transcription shut-off. The blue circles are for cells without Pol II depletion, and the red triangles are for cells with half Pol II depleted. The experimental data are from Ref. [36]. The blue line is a fitting of the experimental data by the RS model ($E^2 = 3.87 \times 10^{-11}$). The red line is the prediction from the RS model for cells with half Pol II depleted without further fitting.

production rate and the reduction of X_p because X_p is still much higher than K_x (Eq. 13): within the accumulation phase, the mRNA production rate is approximately constant. Therefore, X_p initially decreases almost linearly because of the conversion from X_p to X_n due to transcription (Eq. 6). The linear reduction of X_p holds until X_p hits the Michaelis-Menten constant K_x, which leads to a significant decrease in the mRNA production rate (Eq. 13) (Figure S6). Therefore, we can approximate the duration of the accumulation phase as $T_{acc} \approx (X_p - K_x)/(k_{n,bf} f_{dep})$ according to Eq. 6. Here, $k_{n,bf}$ is the mRNA production rate before perturbation. We have taken account of the reduced replenishment rate from X_c to X_p as $(1 - f_{dep})k_{n,bf}$ where f_{dep} is the fraction of depleted X_c (80% in this case). The values of X_c, X_p, and the mRNA production rate then quickly reaches the new steady-state values, after which the mRNA concentration gradually returns to its original value with a relaxation time determined by the mRNA degradation rate, $\delta_m = \beta_m X_c/V_c$ according to Eq. 4. Therefore, the duration of the reversion phase is $T_{rev} \approx V_c/\beta_m X_c$. Figure 4c shows a schematic of this process.

In the above quantitative description, the initial value of the concentration x_p must be far above the parameter K_x (Figure S6). This condition suggests that for WT cells, X_p is generally non-limiting for transcription (but it is still necessary to initiate transcription), in agreement with the observations in budding yeast [16]. We also confirmed that the three phases in the transcription dynamics following an acute depletion are robust against different choices of the parameters (Figure S7). In conclusion, the predictions of the RS model not only perfectly aligned with the experimental data from which we inferred the set of basic parameters (Figure 4a and

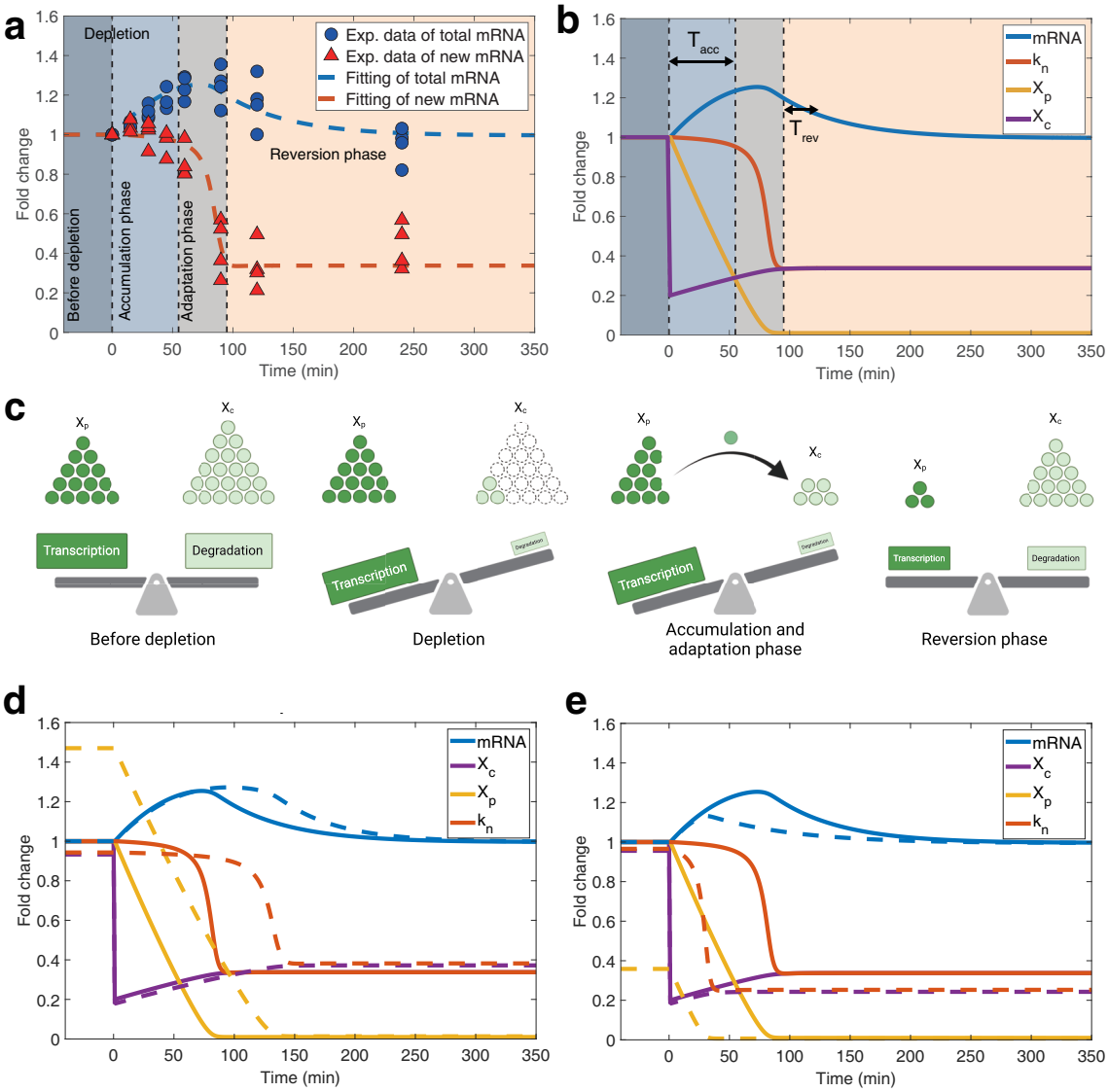

FIG. 4. **The RS model predicts the temporal change of mRNA concentration after an acute perturbation of the degradation factor.** Exp., experiment. (a) The temporal changes in the total mRNA concentration (total mRNA) and recently-transcribed mRNA concentration (new mRNA) following acute depletion of the degradation factor X. The data points represent experimental measurements from [16]. The dashed lines are fitting of the experimental data by optimizing parameters in the RS model ($MSE = 2.10 \times 10^{-3}$). We used the mRNA production rate as a proxy for the recently-transcribed mRNA concentration. (b) Simulation results of the temporal dynamics of mRNA, k_n, X_p, and X_c. (c) The schematic illustrating the dynamics of X after an acute depletion of X_c and its influence on transcription and degradation at different times. (d) Impact of a lower Pol II concentration (a larger K_v) on the temporal changes following depletion of X_c. The solid lines are WT cells, and the dashed lines are for cells with a larger K_v. Both the solid and dashed lines are relative to the values of the WT cells before depletion. (e) Influence of a lower X concentration (a lower X_t) on the temporal changes after depleting X_c. The lines have the same meaning as (d).

Methods) but also provided valuable insights into the underlying mechanism (Figure 4b and c).

Next, we sought to systematically investigate the transcription dynamics after acute depletion of X_c according to the RS model, in particular, considering cells with different concentrations of Pol II or protein X. Future experiments can test our predictions. We compared a WT cell (solid lines in Figure 4d) and a mutant cell with a lower Pol II concentration (dashed lines in Figure 4d). The mutant with a lower Pol II concentration, equivalent to a larger K_v in the RS model, has a mildly lower mRNA production rate than the WT cell. Therefore, the mutant has more X_p, and fewer X_n, X_c (Eqs. 10 and 11). Consequently, it takes longer for the mutant cell to reach

the adaptation phase since it needs a longer time for X_p to decrease and reach the MM constant K_x. Because of the longer duration of the accumulation phase for the mutant, which also has a similar accumulation rate of X_c as the WT cell, the mutant has a higher X_c in the new steady state. Therefore, the mutant recovers more rapidly during the reversion phase than the WT cell.

For the mutant (dashed lines in Figure 4e) with a lower X concentration, it has fewer X_p than the WT cell (solid lines in Figure 4e), but its mRNA production rate remains close to the WT cell as long as the concentration of X_p is still significantly larger than K_x. Because of the fewer X_p, the mutant with a lower X concentration exhibits a shorter accumulation phase than the WT cell. Therefore, the mutant also has a lower number of X_c during the reversion phase, so the mRNA concentration recovers slower in the mutant than in the WT cell. We also investigated the temporal transcription dynamics for other mutants with different modified parameters (Figure S7).

Candidates of X and Y

Experiments showed that the mRNA concentration was buffered even when the global degradation factors such as Dcp2 and Xrn1 were knocked out [8, 16]. These factors play vital roles in 5'-3' mRNA degradation, the predominant pathway of mRNA degradation [32]. These observations suggest that the protein X and Y in the RS model may not represent a single protein, and they may be a combination of multiple proteins. To demonstrate this idea explicitly, we investigated the response of mRNA concentration to an abrupt drop in the mRNA production rate by considering cells with different total numbers of protein X. We found that the recovery time of mRNA concentration diverges in the limit of $X_t \to 0$ (upper panel of Figure 5a). This result suggests that if protein X is only Xrn1, cells with Xrn1 knocked out should not recover from a slight noise in the mRNA production rate, so it cannot achieve mRNA buffering, contradicting experiments. We analyzed protein Y similarly and obtained the same results (lower panel of Figure 5a). Therefore, we proposed that X and Y represent groups of multiple proteins that perform similar functions (Figure 5b).

The necessity of X_p and Y_p to transcription (Figure S2) implies that they must be essential components of the transcription machinery, such as the subunit of Pol II, the general transcription factors, and other necessary molecules. Rpb4 and Rpb7, the subunits of Pol II, are possible candidates involved in shuttling across the nuclear membrane and regulating mRNA degradation [4, 33–35]. Although the cytoplasmic function of Rpb4 is shown to be dispensable [46], similar functions may exist in other factors of the transcription machinery. CDK8, orthologous to budding yeast Ssn3, is a cyclin-dependent kinase (CDK) functional in phosphorylating the CTD of Pol II, promoting the assembly of the elongation complex [47]. Evidence shows that CDK8 participates in the degradation of several mRNAs related to metabolism [48–50]. Hmt1 is a methyltransferase in budding yeast, which participates at the beginning of the transcriptional elongation process and influences mRNA exportation by methylating some RBPs [51]. SUS1 encodes a protein that is a shared subunit of two complexes: Spt-Ada-Gcn5 acetyltransferase (SAGA) and transcription and export complex 2 (TREX-2). SAGA modifies chromatin structure and facilitates transcription initiation, while TREX-2 is a complex that associates with the nuclear pore complex and mediates mRNA export [52]. In a nutshell, we provided a list of candidates of X and Y, participating in at least two of the three processes, including transcription, exportation, and degradation (Table I).

Typically, genetic perturbation methods are used to map a gene to a phenotype of interest. If the knockout or knockdown of a particular gene affects the phenotype, it suggests that the gene is likely responsible for the phenotype. However, in the case of X, which is likely a combination of proteins with redundant functions, perturbing a single gene may not significantly impact mRNA buffering, making it challenging to identify the candidates responsible for mRNA buffering using traditional approaches.

Fortunately, the RS model suggests an alternative solution. We found that the RS model made an interesting prediction if transcription is completely inhibited through Pol II depletion or transcription-inhibiting drugs. In this case, the transformation from X_p to X_n is blocked, while X_n continues to shuttle to the cytoplasm and X_c gradually shuttles back to the nucleus as X_p (Figure 5c). During this process, mRNA continues to be degraded and eventually stabilizes at a lower level (Figure 5c). By monitoring the cytoplasmic proteins that are predominantly transported back to the nucleus after transcription shut-off, one can identify the possible constituents of X (Figure 5d). This prediction of the RS model provides an experimental protocol to examine the potential candidates for X.

Extensions of the RS model

The RS model provides a fundamental understanding of mRNA buffering by revealing the coordination of mRNA production, exportation, and degradation rates to maintain a constant mRNA concentration. However, it is essential to recognize that the real-world dynamics of mRNA regulation can be more complex than the simplified framework of the RS model. This section discusses some of the complexities that may go beyond simplified

TABLE I. Candidates of X and Y in *S. cerevisiae*.

Gene name	Functions as	Gene name	Functions as	Gene name	Functions as	Gene name	Functions as
CAF40	X	MOT2	X	NUP84	Y	SPN1	Y
CCR4	X	NAB2	X and Y	NUP85	Y	SPT6	Y
CDC36	X	NAP1	Y	PHO85	Y	SSL2	Y
CDC39	X	NOT3	X	POP2	X	SSN3	X
CLA4	Y	NOT5	X	RAT1	X	SUS1	X and Y
DCP2	X	NUP100	Y	RMD9	X	THO2	Y
HMT1	Y	NUP120	Y	RPB4	X and Y	UTP8	Y
HPR1	Y	NUP133	Y	RPB7	X	UTP9	Y
HTZ1	X	NUP145	Y	RSP5	Y	WTM1	Y
ISW1	Y	NUP159	Y	RTG2	Y	XRN1	X
MGA2	X	NUP42	Y	SEC13	Y	YAR1	Y
MLP2	Y	NUP53	Y	SGF73	Y	YGR122W	X

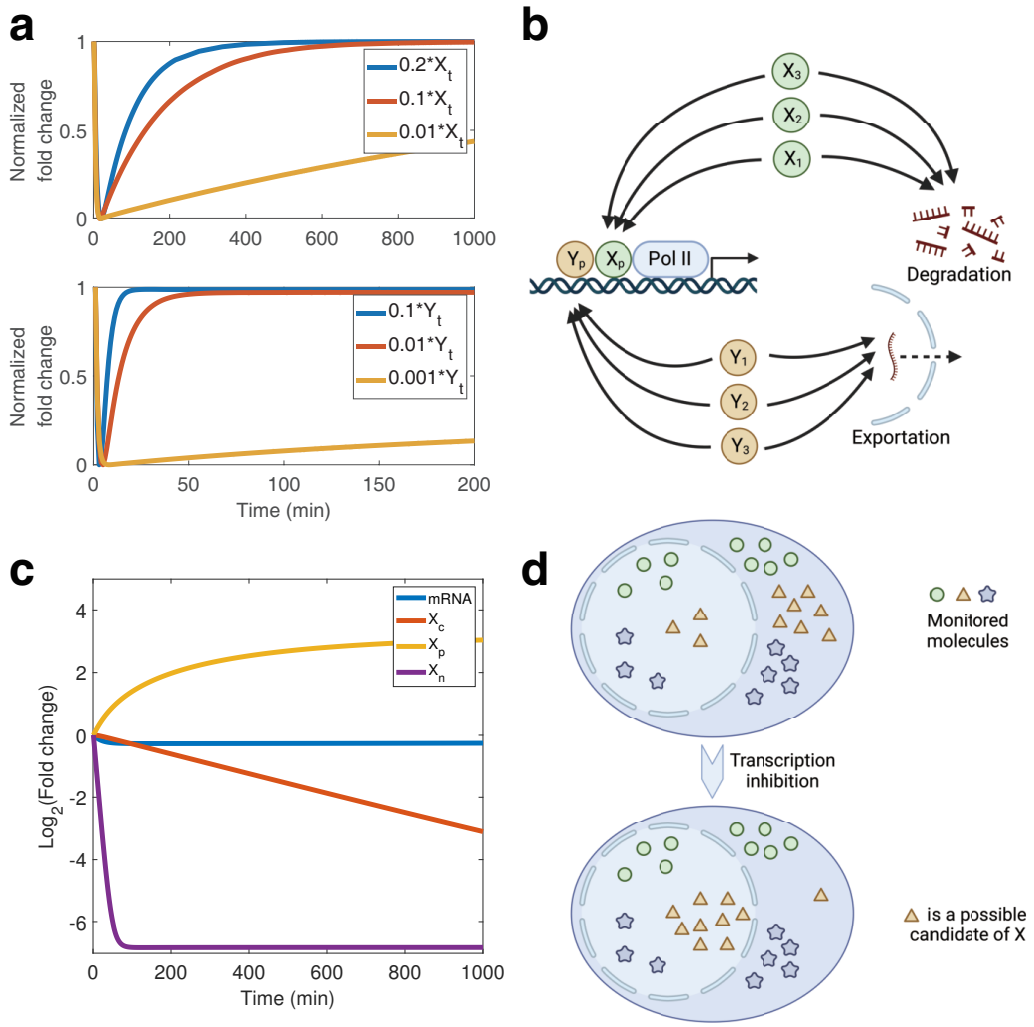

FIG. 5. **Proteins X and Y should represent groups of proteins with similar functions.** (a) The recovery of cytoplasmic mRNA (upper panel with varying copy numbers of X) and nuclear mRNA (lower panel with varying copy numbers of Y) after a rapid perturbation to the mRNA production rate. The y-axis is shifted and normalized so that the value before perturbation is one and the minimum value is 0. (b) Schematic illustrating X and Y can be groups of different proteins executing similar functions. (c) The time course of the mRNA concentration, X_c, X_p, and X_n after the complete shutoff of transcription. (d) Protein X in the cytoplasm will gradually shuttle to the nucleus until most of its copies are localized in the nucleus after a complete transcription inhibition, which can be used to detect the candidates of protein X.

scenario of mRNA buffering and how the RS model can be adapted to address them.

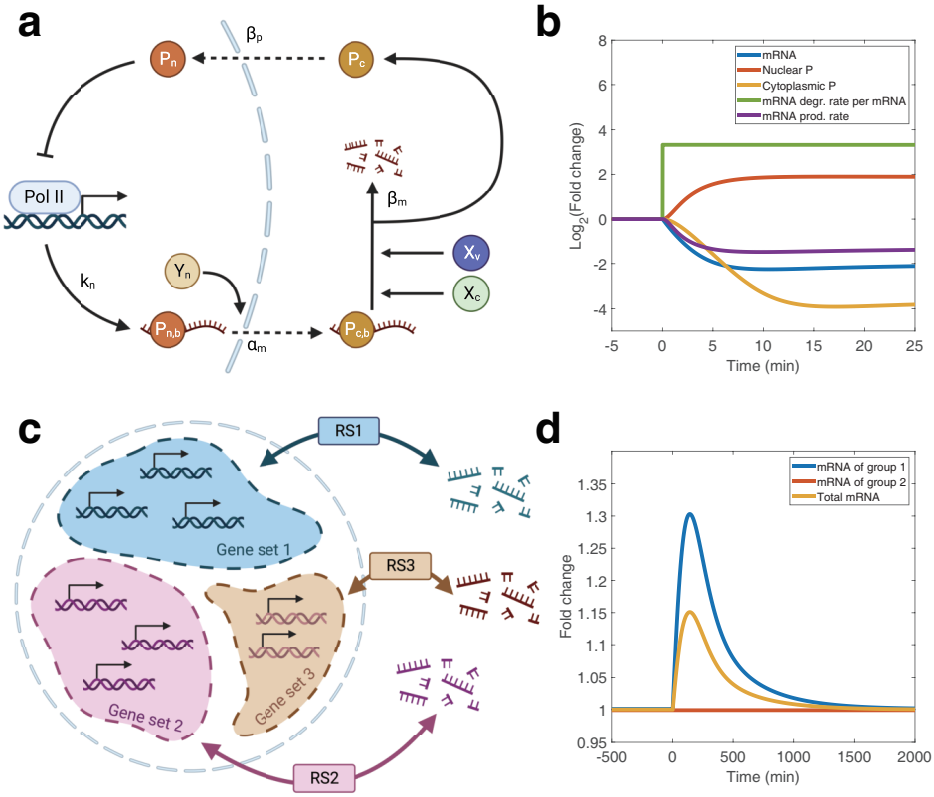

FIG. 6. **The extensions of the RS model.** Degr., degradation; prod., production. (a) Schematic of the modified model in which a third protein P is added. X_v represents the viral endonuclease that increases the factor β_m. (b) Simulations of the dynamics of the mRNA levels, nuclear P ($P_n + P_{n,b}$), cytoplasmic P ($P_c + P_{c,b}$), degradation rates per mRNA, and production rates after a sudden increment of β_m at time 0. (c) Schematic of the generalized model in which different sets of genes are regulated by different groups of X and Y, e.g., RS1, to buffer mRNA concentration separately. (d) Simulations of the dynamics of two groups of mRNA regulated by distinct groups of X and Y and their sum after a sudden decrement in X_c of group 1 at time 0.

We first discuss the mRNA dynamics during viral infection. When cells are infected, the mRNA degradation rates are enhanced to facilitate the rapid turnover of host mRNA and redirect cellular resources toward viral replication, a phenomenon called "host shutoff" [53]. In opposition to the principles of mRNA buffering, although the mRNA degradation rate is accelerated by viral infection, the mRNA production rate becomes slower [54]. Recently, Gilbertson et al. showed that in mammalian cells, the poly(A)-binding protein cytoplasmic 1 (PABPC1) plays a critical role in this process [14]. PABPC1 is an RBP that binds directly to the poly(A) tail of the pre-mRNA in the nucleus and is released in the cytoplasm after mRNA is degraded, functioning in mRNA translation and degradation [55–57]. Researchers found that it also interferes with the formation of PIC in the nucleus [14]. Once the viral endonuclease accelerates mRNA degradation, more PABPC1 proteins are released into the cytoplasm, which then shuttle to the nucleus and inhibit transcription [14]. With this experimental evidence, we modified the RS model by adding a third protein P representing PABPC1 (Figure 6a and Methods). In this modified model, there are four states of P, including the one binding to the nuclear mRNA ($P_{n,b}$), the one binding to the cytoplasmic mRNA ($P_{c,b}$), the free P in the nucleus (P_n), and the free P in the cytoplasm (P_c). We assumed that P binds mRNA tightly and gets released only if the mRNA is degraded so that the numbers of $P_{n,b}$ and $P_{c,b}$ are equal to the nuclear mRNA and cytoplasmic mRNA, respectively. $P_{n,b}$ is assumed to be exported along with mRNA, while the rate of P_c shuttling into the nucleus is determined by the factor β_p. We also modeled the inhibitions of P_n to the mRNA production rate as a Hill function. We modeled the effects of viral infection by increasing β_m. Simulations showed that upon viral infection, the mRNA concentration decreases, and the mRNA degradation rate per mRNA increases while the mRNA production rate decreases. In the meantime, protein P is enriched in the nucleus, in agreement with experimental observations during viral infection (Figure 6b, see Methods for the details of the simulations).

Next, we discuss the differential regulations of specific

mRNA groups. In certain cellular contexts, particular groups of mRNA may be subject to distinct regulatory mechanisms [16, 30, 32]. In such cases, separate sets of proteins X and Y can coexist to buffer each group of mRNA independently (Figure 6c), contributing to the overall homeostasis of mRNA concentration. One benefit of independent RS model systems is that the expression changes of one group of genes do not significantly influence other groups. To demonstrate this benefit explicitly, we modified the RS model to accommodate this specific regulatory scenario by introducing two sets of X and Y, regulating two groups of genes. For simplicity, all parameters are the same for both groups. Simulations of this modified RS model show that despite changes in the mRNA concentration in one group after perturbing its X_c, the mRNA concentration of the other group is largely invariant (Figure 6d, see Methods for the details of the simulations).

In summary, while the RS model provides a powerful framework for understanding mRNA buffering, its simplicity also allows for straightforward extensions and adaptations to capture the complexity of mRNA regulation. By incorporating additional regulatory information, the RS model can be tailored to address specific biological contexts and shed light on the diverse regulation mechanisms of mRNA level.

DISCUSSIONS

In this study, we introduced the releasing-shuttling model as a minimal mechanistic framework to explain mRNA buffering, a fascinating phenomenon observed in various organisms where mRNA concentrations remain relatively constant through coupled changes in mRNA production and degradation rates. The RS model incorporates two essential proteins, X and Y, involved in transcription initiation, mRNA exportation, and mRNA degradation. The model demonstrates that the clue of the mRNA production rate is conveyed downstream via X and Y, synchronizing all rates to achieve mRNA buffering. Through mathematical modeling and analysis, we have shown that the RS model not only provides a robust mechanism of mRNA buffering but also makes valuable predictions that are testable in future experiments. The RS model also allows us to study mRNA homeostasis during cell growth. The model predicts that mRNA concentrations are buffered against changes in cell volume, no matter how the mRNA production rate depends on cell volume. Meanwhile, we noticed that the concentrations of mRNA and protein decrease in budding yeast cells with extremely large sizes [58], which may be due to the imbalance of biomass production and osmolyte synthesis [59, 60].

The RS model also quantitatively predicts the mRNA dynamics following the rapid depletion of protein X. In particular, the RS model predicts a rapid drop in mRNA degradation rate but a relatively constant mRNA production rate in the accumulation phase followed by the adaptation phase and then the reversion phase in which the mRNA concentration decreases exponentially. The RS model perfectly aligns with the experimental observations. It further systematically quantifies the timescales of different phases.

An intriguing aspect of the RS model is the possibility that proteins X and Y may be groups of molecules with redundant functions, providing a plausible explanation for the robustness of mRNA buffering in the face of individual protein perturbations. It is important to note that the precise identity of proteins X and Y in different organisms and cell types remains an open question. We provide a list of candidates for these proteins in budding yeast, including subunits of RNA polymerase II (Pol II), general transcription factors, and proteins involved in mRNA export and degradation (Table I). Specifically for X, the RS model provides an experimental testable method to examine the candidate. Future experiments can utilize the RS model's predictions to identify the specific proteins responsible for mRNA buffering in different cellular contexts.

The RS model also shows flexibility for extensions to capture complexities in biological systems. By incorporating an additional protein, the RS model successfully predicts opposite changes in the mRNA production rate and degradation rate during the viral infection, in contrast to mRNA buffering under other conditions. In addition, separate sets of RS model systems can coexist. These examples highlight the versatility of the RS model in capturing complex regulatory scenarios.

While the RS model successfully explains mRNA buffering and makes valuable predictions, it also raises important questions and opportunities for further investigation. For instance, disruption of the nuclear localization sequence (NLS) of Xrn1 (i.e., inhibiting its shuttling into the nucleus) reduces the transcription rate but also reduces the degradation rate of Kis mRNA, the type of mRNA whose production and degradation are influenced by the disruption of NLS of Xrn1 according to the definition in Ref. [30]. However, non-Kis mRNA's production and degradation rate are not affected by the blocking of Xrn1 import. Meanwhile, the RS model predicts a higher mRNA degradation rate if Xrn1 import is blocked, suggesting that Xrn1 may not be limiting for the classical decay pathway. A possible origin for the different types of mRNA was also proposed: Xrn1 selectively binds to different mRNAs with heterogeneous affinities after they are produced in the nucleus [30]. Further quantitative data are needed to explore the underlying principles and guide the RS model's modification.

In conclusion, the RS model provides a valuable framework for understanding the fundamental regulatory mechanism that ensures mRNA homeostasis. The model

quantitatively explains multiple experimental observations of mRNA buffering and generates novel predictions that can be experimentally tested. As we unravel the complexities of gene expression regulation, the RS model is a valuable tool for guiding future studies and advancing our understanding of transcription regulation.

METHODS

The modified model for the viral infection

To explain the experimental observations of the viral infection, we added another protein, P, to the RS model, representing protein PABPC1 (Figure 6a). The dynamics of P follows

$$\frac{dP_{n,b}}{dt} = k_n - \beta_p P_c, \tag{14}$$

$$\frac{dP_{n,c}}{dt} = \alpha_m \frac{Y_n}{V_n} P_{n,b} - \beta_m \frac{X_c}{V_c} P_{n,c}, \tag{15}$$

$$\frac{dP_c}{dt} = \beta_m \frac{X_c}{V_c} P_{n,c} - \beta_p P_c, \tag{16}$$

$$\frac{dP_n}{dt} = \beta_p P_c - k_n. \tag{17}$$

Here $P_{n,b} = m_n$ and $P_{c,b} = m_c$ because P binds to mRNA tightly. To model the inhibition of PABPC1 to transcription, we included P_n to Eq. 13, so that

$$k_n = k_0 \frac{V_n}{V_n + K_v} \frac{x_p}{x_p + K_x} \frac{y_p}{y_p + K_y} \frac{K_m}{c_{m,n} + K_m} \frac{K_p}{p_n + K_p}, \tag{18}$$

where p_n is the concentration of P_n in nucleus, and K_p is a constant.

Analysis of experimental data

In Figure 2a, b, the experimental data were obtained from [19]. The nuclear mRNA concentrations, cytoplasmic mRNA concentrations, and mRNA production rates were calculated by averaging the "mean nucleus mean FISH," "mean cytoplasm mean FISH," and "mean nucleus mean EU" values, respectively, across all samples perturbing the same gene (or scrambled pieces). The data were then normalized by the mean values of the scrambled samples to obtain fold changes.

In Figure 3e, the experimental data for WT cells and cells with half of the Pol II depleted were obtained from Supplementary Figure 8e of [36]. We set the time point at 6 minutes as the starting time point, the values of which were set to 1. Only the data after the starting time point were used. We then fitted the data of WT cells with a one-phase exponential decay model to get the degradation rates per mRNA ($r^2 = 0.97$).

In Figure 4a, the experimental data were obtained from the supplementary table "xrn1 global nas traj repeats" in [16]. mRNA levels were obtained from "smoothed mRNA", and newly transcribed mRNA levels were obtained from "nascent". All values were normalized with the corresponding values at time 0 to obtain fold changes.

Determination of basic parameters

In the RS model, there are a total of 14 unknown parameters: k_0, K_x, K_y, K_m, K_v, α_m, α_x, α_y, β_m, β_x, X_t, Y_t, V_n, and V_c. Exploring the entire parameter space to find combinations that quantitatively fit the experimental data is a complex task due to the large number of parameters involved. Therefore, we fixed some parameters within biologically reasonable ranges to simplify the analysis and made some assumptions. More quantitative experiments are necessary to refine the parameters and improve our understanding of the RS model in the future.

We assumed a total cell volume of 40 fL, the typical volume of haploid *S. Saccharomyces*. Since the nuclear volume is approximately 7% of the total cell volume [61], we set the nuclear volume (V_n) to 2.8 fL and the cytoplasmic volume (V_c) to 37.2 fL. Throughout the simulations, the values of V_n and V_c are kept fixed, except for the simulations involving cell growth (Figure 3b, c, and d), where the ratio between V_n and V_c is maintained while the cell volume increases.

To estimate the value of K_v, we assumed that the influence on the mRNA production rate k_n (Eq. 13) is primarily determined by the term $V_n/(V_n + K_v)$ when the cell volume increases, which we confirmed numerically (Figure S5). We calculated the fold changes of mRNA production rates (FC_{k_n}) in cells with different volumes as

$$FC_{k_n} = \frac{V_n(V_{n,0} + K_v)}{V_{n,0}(V_n + K_v)}, \tag{19}$$

where $V_{n,0}$ is the reference nuclear volume. We fit this equation to the experimental data from [36] to determine the value of K_v (Figure 3b).

We performed a fitting process to determine the remaining 11 parameters using experimental data from [16]. First, we realized it was challenging to find the optimal fitting parameters by directly fitting the experimental data to the RS model since there are 11 degrees of freedom. Therefore, we searched the optimal fitting parameters starting from the biologically reasonable values inferred from the experimental data. We used the following lower indexes to indicate the values of different factors at different phases of Xrn1 depletion: "bf" (before depletion), "1"(start of the accumulation phase), "acc" (during the accumulation phase), "2"(start of the adaptation phase), "adp" (during the adaptation phase), "3" (start of the reversion phase), and "rev" (during the

reversion phase). Figure S8 shows a schematic of the fitting process.

We assumed that α_y is sufficiently large so that Y_p is virtually proportional to k_n at any given time, i.e., $Y_p \approx k_n/\alpha_y$, which ensures a constant nuclear mRNA concentration (note that if $Y_p = k_n/\alpha_y$, m_n always equals to its steady-state value according to Eq. 1).

Based on the simulations in Figure 4b, we noticed that the excess mRNA is degraded exponentially in the reversion phase since X_c has reached its steady value at the beginning of the reversion phase. Therefore, we fit the data during the reversion phase (after 95 minutes) using the following equation:

$$FC_{m_t} = 1 + ae^{-bt}, \tag{20}$$

where FC_{m_t} represents the fold change of mRNA concentration relative to the value before perturbation at time t, and a and b are the parameters determined by fitting. On the other hand, since the nuclear mRNA concentration is constant throughout the process, the nuclear mRNA export rate always equals k_n. Therefore, we rewrote Eq. 4 as

$$\frac{dm_c}{dt} = k_n - \beta_m \frac{X_c}{V_c} m_c. \tag{21}$$

We then integrated Eq. 21 to obtain the temporal changes in cytoplasmic mRNA:

$$m_{c,rev} = \frac{k_{n,rev} + Ce^{-\delta_{m,rev}t}}{\delta_{m,rev}}, \tag{22}$$

where $m_{c,rev}$ is the cytoplasmic mRNA number during the reversion phase, $k_{n,rev}$ is the mRNA production rate during the reversion phase (which is constant in the reversion phase), and C is a constant. $\delta_{m,rev}$ is the mRNA degradation rate per mRNA so that $\delta_{m,rev} = \beta_m \frac{X_{c,rev}}{V_c}$, where $X_{c,rev}$ is the number of X_c during the reversion phase (which is also constant). Given that the amount of nuclear mRNA remains constant, we expressed the fold change of total mRNA as

$$FC_{m_t} = \frac{m_n + m_{c,rev}}{m_n + m_{c,bf}}, \tag{23}$$

where m_n is the nuclear mRNA number and $m_{c,bf}$ is the cytoplasmic mRNA number before Xrn1 depletion. Using Eqs. 20-23, it is easy to find that $\delta_{m,rev} = b$.

Experimental data showed that $k_{n,rev}$ decreased to approximately 0.4 times the mRNA production rate before perturbation $k_{n,bf}$ (Figure 4a). Therefore, $m_{c,bf} = 0.4k_{n,bf}/\delta_{m,rev}$ because the cytoplasmic mRNA numbers are the same between the steady states before and after the perturbation. Typically, the mRNA production rate of budding yeast cells ranges from about 180 to 2300 mRNA per minute [62]. Hence, we set the mRNA production rate of WT cells before perturbation $k_{n,bf} = 500$ min^{-1}, from which we determined the value of $m_{c,bf}$.

We focused on the accumulation and adaptation phases to estimate the remaining parameters' values. We rewrote Eq. 13 as:

$$k_n = k_0' \frac{X_p}{X_p + K_x'}, \tag{24}$$

where $K_x' = K_x V_n$, and $k_0' = k_0 \frac{V_n}{V_n + K_v} \frac{y_p}{y_p + K_y} \frac{K_m}{c_{m,n} + K_m}$. We assumed that k_0' is almost constant throughout the process so that the mRNA production rate k_n (Eq. 13) is approximately proportional to $X_p/(X_p + K_x')$ during the depletion experiment of Xrn1.

Calculating the analytical solutions for the time dependence of X_c and k_n was challenging, particularly for k_n as it depends on X_p. To simplify the problem, we made the following approximations. Simulations in Figure 4b showed that X_c increases approximately linearly in the accumulation and adaptation phases. Therefore, the transformation speed $v_{trans} = \beta_x X_c$ from X_c to X_p is also linear. In the steady state before perturbation, $v_{trans,bf} = k_{n,bf} = \beta_x X_{c,bf}$. At the beginning of the accumulation phase, we assumed that 80% of X_c are depleted so that $X_{c,1} \approx 0.2X_{c,bf}$, therefore $v_{trans,1} \approx 0.2v_{trans,bf}$. Because the mRNA production rate and the transformation rate must balance as well in the steady after perturbation, $v_{trans,rev} = k_{n,rev} = \beta_x X_{c,rev}$. According to the experimental data, $k_{n,3} = k_{n,rev} \approx 0.4k_{n,bf}$ at the end of the adaptation phase, so that $v_{trans,3} = v_{trans,rev} \approx 0.4v_{trans,bf}$. Therefore, we could approximate the transformation rates at any given time for the experimental data by $v_{trans}(t) = v_{trans,1} + \frac{v_{trans,3} - v_{trans,1}}{T_{acc} + T_{adp}} t$. Here, T_{acc} and T_{adp} are the durations of the accumulation and adaptation phases. We also calculated the time-averaged transformation rates in the accumulation phase ($\langle v_{trans,acc} \rangle$) and the adaptation phase ($\langle v_{trans,adp} \rangle$).

Similarly, we approximated the change in k_n in the experimental data with a combination of two linear reductions: a small slope in the accumulation phase and a large slope in the adaptation phase. Likewise, we computed the time-averaged mRNA production rates during these two phases ($\langle k_{n,acc} \rangle$ and $\langle k_{n,adp} \rangle$). With these linear approximations, we calculated the changes in X_p during the accumulation and adaptation phases:

$$X_{p,2} = X_{p,bf} - T_{acc}(\langle k_{n,acc} \rangle - \langle v_{trans,acc} \rangle), \tag{25}$$
$$X_{p,3} = X_{p,2} - T_{adp}(\langle k_{n,adp} \rangle - \langle v_{trans,adp} \rangle), \tag{26}$$

where $X_{p,2}$ and $X_{p,3}$ are the numbers of X_p at the end of the accumulation and adaptation phases, respectively. Based on experimental data, the mRNA production rate at the end of the accumulation phase ($k_{n,2}$) was approximately $0.95k_{n,bf}$, while at the end of the adaptation phase, $k_{n,3}$ was around $0.4k_{n,bf}$. Using Eq. 24, we wrote

following equations:

$$k_{n,1} = k_0' \frac{X_{p,bf}}{X_{p,bf} + K_x'}, \tag{27}$$

$$k_{n,2} = k_0' \frac{X_{p,2}}{X_{p,2} + K_x'}, \tag{28}$$

$$k_{n,3} = k_0' \frac{X_{p,3}}{X_{p,3} + K_x'}. \tag{29}$$

Given that $k_{n,bf} = 500\ \mathrm{min}^{-1}$, we solved the above equations and obtained the values of k_0', K_x', and $X_{p,bf}$.

Next, we numerically calculated the amount of mRNA accumulated during the accumulation and adaptation phases. Using the constant mRNA degradation rate in the reversion phase $\delta_{m,rev} = \beta_m \frac{X_{c,rev}}{V_c}$ and $X_{c,rev} = 0.4X_{c,bf}$, we obtain $\delta_{m,bf} = \delta_{m,rev}/0.4$. We rewrote Eq. 21 as

$$\frac{dm_c}{dt} = k_n - \delta_{m,bf} \frac{X_c}{X_{c,bf}} m_c. \tag{30}$$

Using the linear approximations of k_n and X_c in the accumulation and adaptation phase, we numerically integrated the equation to obtain the total cytoplasmic mRNA $m_{c,3}$ at the end of the adaptation phase, where the total mRNA is approximately $1.3m_{t,bf}$ (Figure 4a). Therefore,

$$1.3 = \frac{m_n + m_{c,3}}{m_n + m_{c,bf}}, \tag{31}$$

from which we solved for the value of m_n.

We have so far obtained the following parameters from the experimental data of [16]: m_c ($m_{c,bf}$), m_n, X_p ($X_{p,bf}$), k_0', K_x', and δ_m ($\delta_{m,bf}$) for a cell without Xrn1 depletion. We next estimated all the parameters as the starting point of the parameter search process. We set $k_0 = 6000\ min^{-1}$, $K_y = 100\ fL^{-1}$, and $Y_p = 1 \times 10^4$ to solve K_m with the definition of k_0'. We set $X_n = 5000$ to solve α_x with Eq. 10. We set $X_c = 2 \times 10^5$ to solve β_x with Eq. 11 and β_m with the definition of δ_m. We set $Y_p = Y_n = 1000$ and solve α_y with Eq. 12. We then solve α_m with Eq. 8. Summing up X_n, X_c, and X_p, we obtained X_t and similarly for Y_t.

Finally, we optimized these 11 parameters to fit the experimental data by minimizing the weighted mean squared error (MSE) between the model predictions and the experimental data of the temporal fold changes of mRNA concentration and the mRNA production rates. This optimized set of parameters is the basic set of parameters used in our simulations (Table II).

TABLE II. The basic set of parameters.

Parameter	Value	Unit
k_0	6000.00	min^{-1}
K_x	180.18	fL^{-1}
K_y	100.00	fL^{-1}
K_m	5086.24	fL^{-1}
K_v	5.83	fL
α_m	3.28×10^{-5}	$fL \cdot min^{-1}$
α_x	0.10	min^{-1}
α_y	0.52	min^{-1}
β_m	9.92×10^{-6}	$fL \cdot min^{-1}$
β_x	2.24×10^{-3}	min^{-1}
X_t	2.30×10^5	-
Y_t	1.10×10^4	-
V_n	2.80	fL
V_c	37.20	fL

Details of numerical calculations

For the simulations of global genetic perturbations (Figure 2d, e, f, and S4), we calculated the steady-state values of mRNA concentrations, mRNA production rates, and mRNA degradation rates using Eqs. 8-12. We randomly sampled all parameters from lognormal distributions for the blue points in Figure 2d, e, f, and S4. The CVs of parameters involved in the expression of k_n, i.e., k_0, K_v, K_x, K_y, V_n, and V_c, were set to 0.5, while the CVs of other parameters were set to 0.2. The total numbers of X and Y were also randomly sampled from lognormal distributions with a CV of 0.5. For the red points in Figure 2d, e, and S4, we randomly sampled α_m from a lognormal distribution with its CV equal to 1, while the CVs of other parameters in the expression of k_n, as well as the total numbers of X and Y, were set to 0.2. In these simulations, we modified k_0 to be 1/8 of the value from the set of basic parameters.

For the simulations involving changing cell volumes (Figure 3b, c, and d), we calculated the steady-state values of the mRNA number, the production rate, and the degradation rate per mRNA given a cell volume. We maintained the same total X and Y concentrations across different volumes. To verify the constant mRNA concentration predicted by the RS model for any volume dependence of the mRNA production rate, we replace the volume-dependence term $V_n/(V_n + K_v)$ in Eq. 13 by $10^{-5}V_n^{1.5}$ in Figure 3c, and $0.05\sqrt{V_n}(\sin(5V_n)+2)$ in Figure 3d. In these simulations, we modified k_0 to be 1/3 of the value from the set of basic parameters.

For the simulations involving perturbations of Pol II numbers (Figure 3e), we monitored the temporal changes in the mRNA concentration of a specific gene under different values of K_v after silencing the expression of that gene. The parameters used in the simulations (except K_v) were optimized from the basic parameters to minimize the squared error (E^2) between the experimental and predicted degradation rates in WT cells (see details in the analysis of experimental data).

For the simulations depicting the temporal changes after acute depletion of Xrn1 (Figure 4a, b, d, e, and S7), we calculated the fold changes of different molecules compared to the respective homeostatic values before deple-

tion. To mimic the acute depletion of Xrn1, we instantaneously removed 80% of X_c from the cytoplasm. In Figure 4d, e, and Figure S7, two simulations are shown together in each plot. All parameters used in these simulations are the same except for the one indicated in each plot.

For the simulations examining temporal changes of mRNA with different concentrations of X or Y (Figure 5a), we monitored the changes of cytoplasmic and nuclear mRNA levels after inhibiting transcription, compared to their values before perturbation. We inhibited transcriptional by instantaneously decreasing the value of k_0 to its 50% at time 0.

For the simulations of temporal changes after complete transcription inhibition (Figure 5c), we introduced a very large K_v to completely shut off transcription at time zero, and then calculated the temporal changes of mRNA and X.

For the simulation of the modified model with additional protein P (Figure 6b), we simulated the temporal changes of the total number of mRNA, the cytoplasmic P ($P_c + P_{c,b}$), the nuclear P ($P_c + P_{c,b}$), the mRNA production rate, and the mRNA degradation rate per mRNA using Eqs. 14-18 after increasing the degradation factor β_m by a factor of 10 at time 0, mimicking the globally accelerated degradation of the host mRNA during the viral infection. In these simulations, we modified α_m to be 20 times of the value from the set of basic parameters.

To simulate the extended model involving several gene-specific RS models (Figure 6d), we simulated the transcription of two groups of genes regulated by their own Xs and Ys. The parameters of these two RS models are set the same. We perturbed the expression of one group of genes by decreasing the number of its X_c to its 10% at time zero. We then monitored the temporal changes of the mRNA concentrations of both groups and the total mRNA concentration.

Finding candidates of X and Y

The RS model suggests that X and Y are multifunctional molecules involved in transcription, exportation, and degradation. To identify candidate genes in these categories, we utilized various databases, including the Gene Ontology (GO) database through AmiGO (version 2.5.17) [63–65], the Kyoto Encyclopedia of Genes and Genomes (KEGG) database [66–68], and the Saccharomyces Genome Database (SGD) [69]. In our search for transcription-related genes, we focused on those annotated as transcription factors or involved in the regulation of transcription, as well as the subunits of Pol II. For exportation-related genes, we looked for annotations related to nuclear transportation factors and the subunits of the nuclear pore. In the context of degradation, we identified genes involved in mRNA catabolism. We marked genes with dual functions in transcription and exportation as Y and genes with dual functions in transcription and degradation as X (Table I).

Data availability

All data are acquired from public repositories. The experimental data of the global genetic perturbations in mammalian cells were obtained from [19]. The experimental data of the global genetic perturbations in budding yeast cells were obtained from [9]. The experimental data of volume changes were obtained from [36]. The mRNA production rate fold changes were obtained from the Pol II occupancy data in Figure 1e of [36]. Figure 6c of [36] shows the fold change of mRNA degradation rate. The experimental data of perturbing Pol II were obtained from Supplementary Figure 8e of [36]. The experimental data of the acute depletion of Xrn1 were obtained from [16].

Code Availability

All codes for mathematical simulations are available in the following link (https://github.com/QirunWang/Codes-for-the-RS-model).

ACKNOWLEDGMENTS

All schematics are created with BioRender.com. The research was funded by National Key R&D Program of China (2021YFF1200500) and supported by grants from Peking-Tsinghua Center for Life Sciences.

COMPETING INTERESTS

The authors declare that there are no competing interests.

[1] K. A. Braun and E. T. Young, Coupling mrna synthesis and decay, Molecular and Cellular Biology **34**, 4078 (2014).

[2] H. T. M. Timmers and L. Tora, Transcript buffering: a balancing act between mrna synthesis and mrna degradation, Molecular cell **72**, 10 (2018).

[3] E. Hartenian and B. A. Glaunsinger, Feedback to the central dogma: cytoplasmic mrna decay and transcription are interdependent processes, Critical reviews in biochemistry and molecular biology **54**, 385 (2019).

[4] O. Shalem, B. Groisman, M. Choder, O. Dahan, and Y. Pilpel, Transcriptome kinetics is governed by a

genome-wide coupling of mrna production and degradation: A role for rna pol ii, PLOS Genetics **7**, 1 (2011).

[5] A. Esberg, Z. Moqtaderi, X. Fan, J. Lu, K. Struhl, and A. Byström, Iwr1 protein is important for preinitiation complex formation by all three nuclear rna polymerases in saccharomyces cerevisiae, PLOS ONE **6**, 1 (2011).

[6] K. Helenius, Y. Yang, T. Tselykh, H. Pessa, M. Frilander, and T. Mäkelä, Requirement of tfiih kinase subunit mat1 for rna pol ii c-terminal domain ser5 phosphorylation, transcription and mrna turnover, Nucleic acids research **39**, 5025 (2011).

[7] M. Sun, B. Schwalb, D. Schulz, N. Pirkl, S. Etzold, L. Larivière, K. Maier, M. Seizl, A. Tresch, and P. Cramer, Comparative dynamic transcriptome analysis (cdta) reveals mutual feedback between mrna synthesis and degradation, Genome research **22**, 1350 (2012).

[8] G. Haimovich, D. A. Medina, S. Z. Causse, M. Garber, G. Millán-Zambrano, O. Barkai, S. Chávez, J. E. Pérez-Ortín, X. Darzacq, and M. Choder, Gene expression is circular: factors for mrna degradation also foster mrna synthesis, Cell **153**, 1000 (2013).

[9] M. Sun, B. Schwalb, N. Pirkl, K. C. Maier, A. Schenk, H. Failmezger, A. Tresch, and P. Cramer, Global analysis of eukaryotic mrna degradation reveals xrn1-dependent buffering of transcript levels, Molecular cell **52**, 52 (2013).

[10] J. Rodríguez-Molina, S. Tseng, S. Simonett, J. Taunton, and A. Ansari, Engineered covalent inactivation of tfiih-kinase reveals an elongation checkpoint and results in widespread mrna stabilization, Molecular Cell **63**, 433 (2016).

[11] T. Baptista, S. Grünberg, N. Minoungou, M. Koster, H. Timmers, S. Hahn, D. Devys, and L. Tora, Saga is a general cofactor for rna polymerase ii transcription, Molecular Cell **68** (2017).

[12] L. Warfield, S. Ramachandran, T. Baptista, D. Devys, L. Tora, and S. Hahn, Transcription of nearly all yeast rna polymerase ii-transcribed genes is dependent on transcription factor tfiid, Molecular Cell **68**, 118 (2017).

[13] V. García-Molinero, J. García-Martínez, R. Reja, P. Furió-Tarí, O. Antúnez, V. Vinayachandran, A. Conesa, B. F. Pugh, J. E. Pérez-Ortín, and S. Rodríguez-Navarro, The saga/trex-2 subunit sus1 binds widely to transcribed genes and affects mrna turnover globally, Epigenetics & Chromatin **11**, 1 (2018).

[14] S. Gilbertson, J. D. Federspiel, E. Hartenian, I. M. Cristea, and B. Glaunsinger, Changes in mrna abundance drive shuttling of rna binding proteins, linking cytoplasmic rna degradation to transcription, eLife **7**, e37663 (2018).

[15] J. Garcia-Martinez, A. Aranda, and J. Perez-Ortin, Genomic run-on evaluates transcription rates for all yeast genes and identifies gene regulatory mechanisms, Molecular cell **15**, 303 (2004).

[16] A. Chappleboim, D. Joseph-Strauss, O. Gershon, and N. Friedman, Transcription feedback dynamics in the wake of cytoplasmic mRNA degradation shutdown, Nucleic Acids Research **50**, 5864 (2022).

[17] P. Singh, R. S. James, C. J. Mee, and I. Y. Morozov, mrna levels are buffered upon knockdown of rna decay and translation factors via adjustment of transcription rates in human hepg2 cells, RNA biology **16**, 1147 (2019).

[18] B. Slobodin, A. Bahat, U. Sehrawat, S. Becker-Herman, B. Zuckerman, A. Weiss, R. Han, R. Elkon, R. Agami, I. Ulitsky, I. Shachar, and R. Dikstein, Transcription dynamics regulate poly(a) tails and expression of the rna degradation machinery to balance mrna levels, Molecular Cell **78** (2020).

[19] S. Berry, M. Müller, A. Rai, and L. Pelkmans, Feedback from nuclear rna on transcription promotes robust rna concentration homeostasis in human cells, Cell Systems **13**, 454 (2022).

[20] O. Padovan-Merhar, G. P. Nair, A. G. Biaesch, A. Mayer, S. Scarfone, S. W. Foley, A. R. Wu, L. S. Churchman, A. Singh, and A. Raj, Single mammalian cells compensate for differences in cellular volume and dna copy number through independent global transcriptional mechanisms, Molecular Cell **58**, 339 (2015).

[21] Y. Chen, G. Zhao, J. Zahumensky, S. Honey, and B. Futcher, Differential scaling of gene expression with cell size may explain size control in budding yeast, Molecular Cell **78**, 359 (2020).

[22] X.-M. Sun, A. Bowman, M. Priestman, F. Bertaux, A. Martinez-Segura, W. Tang, C. Whilding, D. Dormann, V. Shahrezaei, and S. Marguerat, Size-dependent increase in rna polymerase ii initiation rates mediates gene expression scaling with cell size, Current Biology **30**, 1217 (2020).

[23] J. Zhurinsky, K. Leonhard, S. Watt, S. Marguerat, J. Bähler, and P. Nurse, A coordinated global control over cellular transcription, Current Biology **20** (2010).

[24] S. Berry and L. Pelkmans, Mechanisms of cellular mrna transcript homeostasis, Trends in Cell Biology (2022).

[25] J. Lin and A. Amir, Homeostasis of protein and mrna concentrations in growing cells, Nature Communications **9**, 4496 (2018).

[26] Q. Wang and J. Lin, Heterogeneous recruitment abilities to rna polymerases generate nonlinear scaling of gene expression with cell volume, Nature Communications **12** (2021).

[27] M. P. Swaffer, J. Kim, D. Chandler-Brown, M. Langhinrichs, G. K. Marinov, W. J. Greenleaf, A. Kundaje, K. M. Schmoller, and J. M. Skotheim, Transcriptional and chromatin-based partitioning mechanisms uncouple protein scaling from cell size, Molecular Cell **81**, 4861 (2021).

[28] S. Geisler and J. Coller, Chapter five - xrn1: A major 5' to 3' exoribonuclease in eukaryotic cells, in *Eukaryotic RNases and their Partners in RNA Degradation and Biogenesis, Part A*, The Enzymes, Vol. 31, edited by G. F. Chanfreau and F. Tamanoi (Academic Press, 2012) pp. 97–114.

[29] V. K. Nagarajan, C. I. Jones, S. F. Newbury, and P. J. Green, Xrn 5'→3' exoribonucleases: Structure, mechanisms and functions, Biochimica et Biophysica Acta (BBA) - Gene Regulatory Mechanisms **1829**, 590 (2013), rNA Decay Mechanisms.

[30] S. Chattopadhyay, J. Garcia-Martinez, G. Haimovich, J. Fischer, A. Khwaja, O. Barkai, S. G. Chuartzman, M. Schuldiner, R. Elran, M. I. Rosenberg, *et al.*, Rna-controlled nucleocytoplasmic shuttling of mrna decay factors regulates mrna synthesis and a novel mrna decay pathway, Nature communications **13**, 7184 (2022).

[31] M. A. Collart, The ccr4-not complex is a key regulator of eukaryotic gene expression, WIREs RNA **7**, 438 (2016).

[32] K. A. Braun and E. T. Young, Coupling mrna synthesis and decay, Molecular and Cellular Biology **34**, 4078 (2014).

[33] V. Goler-Baron, M. Selitrennik, O. Barkai, G. Haimovich, R. Lotan, and M. Choder, Transcription in the nucleus and mrna decay in the cytoplasm are coupled processes, Genes & development **22**, 2022 (2008).

[34] L. Harel-Sharvit, N. Eldad, G. Haimovich, O. Barkai, L. Duek, and M. Choder, Rna polymerase ii subunits link transcription and mrna decay to translation, Cell **143**, 552 (2010).

[35] M. Choder, mrna imprinting, Cellular logistics **1**, 37 (2011).

[36] M. P. Swaffer, G. K. Marinov, H. Zheng, C. Y. Tsui, A. W. Jones, J. Greenwood, A. Kundaje, W. J. Greenleaf, R. Reyes-Lamothe, and J. M. Skotheim, Rna polymerase ii dynamics and mrna stability feedback scale mrna in proportion to cell size, bioRxiv 10.1101/2021.09.20.461005 (2022).

[37] D. L. Bentley, Rules of engagement: co-transcriptional recruitment of pre-mrna processing factors, Current Opinion in Cell Biology **17**, 251 (2005), nucleus and gene expression.

[38] H. Feng, H. Tian, Y. Wang, Q. Zhang, N. Lin, S. Liu, Y. Yu, H. Deng, and P. Gao, Molecular mechanism underlying selective inhibition of mrna nuclear export by herpesvirus protein orf10, Proceedings of the National Academy of Sciences **117**, 26719 (2020).

[39] G. Zhang, H. Luo, X. Li, Z. Hu, and Q. Wang, The dynamic poly(a) tail acts as a signal hub in mrna metabolism, Cells **12**, 10.3390/cells12040572 (2023).

[40] K. Tokunaga, T. Shibuya, Y. Ishihama, H. Tadakuma, M. Ide, M. Yoshida, T. Funatsu, Y. Ohshima, and T. Tani, Nucleocytoplasmic transport of fluorescent mrna in living mammalian cells: nuclear mrna export is coupled to ongoing gene transcription, Genes to Cells **11**, 305 (2006).

[41] F. R. Neumann and P. Nurse, Nuclear size control in fission yeast, The Journal of Cell Biology **179**, 593 (2007).

[42] J. E. Henninger, O. Oksuz, K. Shrinivas, I. Sagi, G. LeRoy, M. M. Zheng, J. O. Andrews, A. V. Zamudio, C. Lazaris, N. M. Hannett, *et al.*, Rna-mediated feedback control of transcriptional condensates, Cell **184**, 207 (2021).

[43] R. Reed, Coupling transcription, splicing and mrna export, Current Opinion in Cell Biology **15**, 326 (2003).

[44] M. C. Lanz, E. Zatulovskiy, M. P. Swaffer, L. Zhang, I. Ilerten, S. Zhang, D. S. You, G. Marinov, P. McAlpine, J. E. Elias, *et al.*, Increasing cell size remodels the proteome and promotes senescence, Molecular cell **82**, 3255 (2022).

[45] W.-D. Heyer, A. W. Johnson, U. Reinhart, and R. D. Kolodner, Regulation and intracellular localization of saccharomyces cerevisiae strand exchange protein 1 (sep1/xrn1/kem1), a multifunctional exonuclease, Molecular and Cellular Biology **15**, 2728 (1995), pMID: 7739553.

[46] D. Schulz, N. Pirkl, E. Lehmann, and P. Cramer, Rpb4 subunit functions mainly in mrna synthesis by rna polymerase ii, Journal of Biological Chemistry **289**, 17446 (2014).

[47] A. J. Donner, C. C. Ebmeier, D. J. Taatjes, and J. M. Espinosa, Cdk8 is a positive regulator of transcriptional elongation within the serum response network, Nature structural & molecular biology **17**, 194 (2010).

[48] R. T. Surosky, R. Strich, and R. E. Esposito, The yeast ume5 gene regulates the stability of meiotic mrnas in response to glucose, Molecular and Cellular Biology **14**, 3446 (1994).

[49] G. P. Cereghino and I. E. Scheffler, Genetic analysis of glucose regulation in saccharomyces cerevisiae: control of transcription versus mrna turnover., The EMBO Journal **15**, 363 (1996).

[50] Z. Yin, L. Hatton, and A. J. P. Brown, Differential post-transcriptional regulation of yeast mrnas in response to high and low glucose concentrations, Molecular Microbiology **35**, 553 (2000).

[51] C. Y. Michael, F. Bachand, A. E. McBride, S. Komili, J. M. Casolari, and P. A. Silver, Arginine methyltransferase affects interactions and recruitment of mrna processing and export factors, Genes & development **18**, 2024 (2004).

[52] P. Pascual-García and S. Rodríguez-Navarro, A tale of coupling, sus1 function in transcription and mrna export, RNA Biology **6**, 141 (2009).

[53] T. He, M. Wang, A. Cheng, Q. Yang, Y. Wu, R. Jia, M. Liu, D. Zhu, S. Chen, S. Zhang, *et al.*, Host shutoff activity of vhs and sox-like proteins: role in viral survival and immune evasion, Virology journal **17**, 1 (2020).

[54] E. Abernathy, S. Gilbertson, R. Alla, and B. Glaunsinger, Viral nucleases induce an mrna degradation-transcription feedback loop in mammalian cells, Cell host & microbe **18**, 243 (2015).

[55] N. Hosoda, F. Lejeune, and L. E. Maquat, Evidence that poly(a) binding protein c1 binds nuclear pre-mrna poly(a) tails, Molecular and Cellular Biology **26**, 3085 (2006), pMID: 16581783.

[56] C. Duncan-Lewis, E. Hartenian, V. King, and B. A. Glaunsinger, Cytoplasmic mrna decay represses rna polymerase ii transcription during early apoptosis, eLife **10**, e58342 (2021).

[57] Y. Qi, M. Wang, and Q. Jiang, Pabpc1——mrna stability, protein translation and tumorigenesis, Frontiers in Oncology **12**, 1025291 (2022).

[58] G. E. Neurohr, R. L. Terry, J. Lengefeld, M. Bonney, G. P. Brittingham, F. Moretto, T. P. Miettinen, L. P. Vaites, L. M. Soares, J. A. Paulo, *et al.*, Excessive cell growth causes cytoplasm dilution and contributes to senescence, Cell **176**, 1083 (2019).

[59] R. Rollin, J.-F. Joanny, and P. Sens, Physical basis of the cell size scaling laws, eLife **12**, e82490 (2023).

[60] Y. Ye and J. Lin, Cell size: Putting scaling laws on a physical foundation, eLife **12**, e89415 (2023).

[61] P. Jorgensen, N. P. Edgington, B. L. Schneider, I. Rupeš, M. Tyers, and B. Futcher, The size of the nucleus increases as yeast cells grow, Molecular Biology of the Cell **18**, 3523 (2007), pMID: 17596521.

[62] V. Pelechano, S. Chávez, and J. E. Pérez-Ortín, A complete set of nascent transcription rates for yeast genes, PLOS ONE **5**, 1 (2010).

[63] M. Ashburner, C. A. Ball, J. A. Blake, D. Botstein, H. Butler, J. M. Cherry, A. P. Davis, K. Dolinski, S. S. Dwight, J. T. Eppig, M. A. Harris, D. P. Hill, L. Issel-Tarver, A. Kasarskis, S. Lewis, J. C. Matese, J. E. Richardson, M. Ringwald, G. M. Rubin, and G. Sherlock, Gene ontology: tool for the unification of biology, Nature Genetics **25**, 25 (2000).

[64] S. Carbon, A. Ireland, C. J. Mungall, S. Shu, B. Marshall, S. Lewis, and and, AmiGO: online access to ontology and

annotation data, Bioinformatics **25**, 288 (2008).

[65] S. Carbon, E. Douglass, B. M. Good, D. R. Unni, N. L. Harris, C. J. Mungall, S. Basu, R. L. Chisholm, R. J. Dodson, E. Hartline, P. Fey, P. D. Thomas, L.-P. Albou, D. Ebert, M. J. Kesling, H. Mi, A. Muruganujan, X. Huang, T. Mushayahama, S. A. LaBonte, D. A. Siegele, G. Antonazzo, H. Attrill, N. H. Brown, P. Garapati, S. J. Marygold, V. Trovisco, G. dos Santos, K. Falls, C. Tabone, P. Zhou, J. L. Goodman, V. B. Strelets, J. Thurmond, P. Garmiri, R. Ishtiaq, M. Rodríguez-López, M. L. Acencio, M. Kuiper, A. Lægreid, C. Logie, R. C. Lovering, B. Kramarz, S. C. C. Saverimuttu, S. M. Pinheiro, H. Gunn, R. Su, K. E. Thurlow, M. Chibucos, M. Giglio, S. Nadendla, J. Munro, R. Jackson, M. J. Duesbury, N. Del-Toro, B. H. M. Meldal, K. Paneerselvam, L. Perfetto, P. Porras, S. Orchard, A. Shrivastava, H.-Y. Chang, R. D. Finn, A. L. Mitchell, N. D. Rawlings, L. Richardson, A. Sangrador-Vegas, J. A. Blake, K. R. Christie, M. E. Dolan, H. J. Drabkin, D. P. Hill, L. Ni, D. M. Sitnikov, M. A. Harris, S. G. Oliver, K. Rutherford, V. Wood, J. Hayles, J. Bähler, E. R. Bolton, J. L. D. Pons, M. R. Dwinell, G. T. Hayman, M. L. Kaldunski, A. E. Kwitek, S. J. F. Laulederkind, C. Plasterer, M. A. Tutaj, M. Vedi, S.-J. Wang, P. D'Eustachio, L. Matthews, J. P. Balhoff, S. A. Aleksander, M. J. Alexander, J. M. Cherry, S. R. Engel, F. Gondwe, K. Karra, S. R. Miyasato, R. S. Nash, M. Simison, M. S. Skrzypek, S. Weng, E. D. Wong, M. Feuermann, P. Gaudet, A. Morgat, E. Bakker, T. Z. Berardini, L. Reiser, S. Subramaniam, E. Huala, C. N. Arighi, A. Auchincloss, K. Axelsen, G. Argoud-Puy, A. Bateman, M.-C. Blatter, E. Boutet, E. Bowler, L. Breuza, A. Bridge, R. Britto, H. Bye-A-Jee, C. C. Casas, E. Coudert, P. Denny, A. Estreicher, M. L. Famiglietti, G. Georghiou, A. Gos, N. Gruaz-Gumowski, E. Hatton-Ellis, C. Hulo, A. Ignatchenko, F. Jungo, K. Laiho, P. L. Mercier, D. Lieberherr, A. Lock, Y. Lussi, A. MacDougall, M. Magrane, M. J. Martin, P. Masson, D. A. Natale, N. Hyka-Nouspikel, S. Orchard, I. Pedruzzi, L. Pourcel, S. Poux, S. Pundir, C. Rivoire, E. Speretta, S. Sundaram, N. Tyagi, K. Warner, R. Zaru, C. H. Wu, A. D. Diehl, J. N. Chan, C. Grove, R. Y. N. Lee, H.-M. Muller, D. Raciti, K. V. Auken, P. W. Sternberg, M. Berriman, M. Paulini, K. Howe, S. Gao, A. Wright, L. Stein, D. G. Howe, S. Toro, M. Westerfield, P. Jaiswal, L. Cooper, and J. Elser, The gene ontology resource: enriching a GOld mine, Nucleic Acids Research **49**, D325 (2020).

[66] M. Kanehisa, KEGG: Kyoto encyclopedia of genes and genomes, Nucleic Acids Research **28**, 27 (2000).

[67] M. Kanehisa, Toward understanding the origin and evolution of cellular organisms, Protein Science **28**, 1947 (2019).

[68] M. Kanehisa, M. Furumichi, Y. Sato, M. Ishiguro-Watanabe, and M. Tanabe, KEGG: integrating viruses and cellular organisms, Nucleic Acids Research **49**, D545 (2020).

[69] J. M. Cherry, E. L. Hong, C. Amundsen, R. Balakrishnan, G. Binkley, E. T. Chan, K. R. Christie, M. C. Costanzo, S. S. Dwight, S. R. Engel, D. G. Fisk, J. E. Hirschman, B. C. Hitz, K. Karra, C. J. Krieger, S. R. Miyasato, R. S. Nash, J. Park, M. S. Skrzypek, M. Simison, S. Weng, and E. D. Wong, Saccharomyces Genome Database: the genomics resource of budding yeast, Nucleic Acids Research **40**, D700 (2011).